Check for updates

ChemElectroChem

Research Article
doi.org/10.1002/celc.202300192

Chemistry Europe
European Chemical Societies Publishing

www.chemelectrochem.org

$KFe(C_2O_4)F$: A Fluoro-oxalate Cathode Material for Li/Na-Ion Batteries

Atin Pramanik,[a] Alexis G. Manche,[a, d] Megan T. Smeaton,[a] Moulay-Tahar Sougrati,[b, c] Philip Lightfoot,[a] and Anthony Robert Armstrong*[a, c, d]

The iron-based polyanionic fluoro-oxalate material, $KFe(C_2O_4)F$ (KFCF), has been synthesized by hydrothermal methods. This compound shows promising reversible lithium and sodium insertion properties as a cathode material. The material delivered a first-cycle discharge capacity of 120 $mAh\,g^{-1}$ at ~3.3 V (Li^+/Li) and 97.4 $mAh\,g^{-1}$ at ~3.0 V (Na^+/Na) in LIB and NIB, respectively. Stable cycling performance was observed in both cases. The involvement of reversible Fe^{2+}/Fe^{3+} redox was confirmed by *ex-situ* Mössbauer spectroscopy supported by first-principles calculations. This study reveals promising performance from a mixed oxalate-fluoride based polyanionic material thereby opening up further possibilities for materials discovery in the design of new electrode materials.

Introduction

The continuously increasing global population requires more power, but it is now recognized that fossil fuels must be removed from the generation equation. In addition, concerns about climate change and pollution have triggered countries worldwide to turn to renewable sources for a more significant percentage of their energy needs. However, renewable energy sources such as wind and solar are intermittent, leading to a requirement for backup energy storage such as battery technology. Lithium-ion batteries (LIBs) have been favored due to their high energy density and working voltages, but there are serious concerns due to rising costs.[1] This has led to growing interest in more sustainable battery technologies such as sodium-ion (NIBs), as sodium is highly abundant and much cheaper.[2] In the search for positive electrode materials, layered transition metal oxides and a range of polyanionic materials (phosphate, sulfate, silicate, borate) have been explored, e.g., $NaTMO_2$,[3a] $NaTMPO_4$ (TM = transition metal),[3b] $Na_4Fe_3(PO_4)_2(P_2O_7)$,[3c] $Na_2Fe_2(SO_4)_2$,[3d] Na_2FeSiO_4[3e–g] The polyanionic compounds form strong covalent bonds that enhance stability and improve safety features.

Oxalic acid is also a strong acid ($pK_\alpha = 1.25/4.14$), lying between phosphate and sulfate in terms of acidity. This indicates that the electronic inductive effect of the $(C_2O_4)^{2-}$ should be comparable to $(SO_4)^{2-}$ and $(PO_4)^{3-}$ towards the d-states of the transition metal ions, leading to similar redox potentials. The oxalate anion coordinates with the metal centers via oxygen atoms, forming mono- or poly-nuclear metal complexes. To date, a number of iron-based electrochemically active polyanionic oxalate compounds have been reported, such as $Na_2Fe_2(C_2O_4)_3\cdot 2H_2O$,[4a] $Li_2Fe(C_2O_4)_2$,[4b] $K_2Fe(C_2O_4)_2$,[4c] $KLi_3Fe(C_2O_4)_3$,[4d] $Na_2Fe(C_2O_4)(HPO_4)$,[4e] and $Na_2Fe(C_2O_4)SO_4\cdot H_2O$.[4f] Combining different anion sublattices in a polyanionic system in which the crystal structure was varied with different chemical composition has been found to offer tunable electrochemical activity.[5] Incorporation of fluorine is expected to increase the operating potential due to the higher ionicity of the metal-fluoride bond, resulting in higher energy density. Bearing these considerations in mind, researchers have synthesized various electrochemically active phosphate and sulfate-based mixed metal fluoride compounds such as $AVPO_4F$ (A = Li, Na, K),[6a] $Na_3V_2O_2(PO_4)_2F$,[6b] $LiFePO_4F$, $LiFeSO_4F$, $NaMSO_4F$ (M = Fe, Co, Ni, Mn, Mg, Zn, Cu), and $NaMSO_4F\cdot 2H_2O$ (M = Fe, Co, Ni, Zn) etc.[6c]

Only two electrochemically active oxalate-fluoride complexes have been reported, $Na_2Fe(C_2O_4)F_2$,[7a] and $KFe(C_2O_4)F$.[7b] $Na_2Fe(C_2O_4)F_2$ is electrochemically active in both lithium and sodium ion batteries with average potentials of ~3.3 and 3.0 V, respectively and good cycling stability. Tang et al. reported $KFe(C_2O_4)F$ as a potassium-ion battery (KIB) cathode material with a discharge capacity of 112 $mAh\,g^{-1}$ at an average potential of ~3.2 V.[8] The compound exhibits reversible iron redox ($Fe^{2+}/Fe^{/3+}$) during charge/discharge. However, to date, this material has not been explored as an electrode for LIB/NIB.

[a] *Dr. A. Pramanik, A. G. Manche, M. T. Smeaton, Prof. P. Lightfoot, Dr. A. R. Armstrong*
School of Chemistry
University of St-Andrews
St-Andrews, Fife, KY16 9ST (United Kingdom)
E-mail: ara@st-andrews.ac.uk
Homepage: https://aragroup.wp.st-andrews.ac.uk/
[b] *Dr. M.-T. Sougrati*
Institute Charles Gerhardt
Université de Montpellier
2 Place Eugène Bataillon – CC 1502, 34095 Montpellier Cedex 5 (France)
[c] *Dr. M.-T. Sougrati, Dr. A. R. Armstrong*
Hub de l'énergie, rue Baudelocque, 80039 Amiens Cedex (France)
[d] *A. G. Manche, Dr. A. R. Armstrong*
The Faraday Institution
Quad One
Harwell Science and Innovation Campus
Didcot, OX11 0RA (United Kingdom)

Supporting information for this article is available on the WWW under https://doi.org/10.1002/celc.202300192

© 2023 The Authors. ChemElectroChem published by Wiley-VCH GmbH. This is an open access article under the terms of the Creative Commons Attribution License, which permits use, distribution and reproduction in any medium, provided the original work is properly cited.

© 2023 The Authors. ChemElectroChem published by Wiley-VCH GmbH

21960216, 0, Downloaded from https://chemistry-europe.onlinelibrary.wiley.com/doi/10.1002/celc.202300192 by NHS Education for Scotland NES, Edinburgh Central Office, Wiley Online Library on [28/06/2023]. See the Terms and Conditions (https://onlinelibrary.wiley.com/terms-and-conditions) on Wiley Online Library for rules of use; OA articles are governed by the applicable Creative Commons License

Inspired by these considerations, we prepared $KFe(C_2O_4)F$ hydrothermally and tested its properties as an electrode material in lithium-ion and sodium-ion batteries. We demonstrate that reversible iron redox (Fe^{2+}/Fe^{3+}) occurs during the charge/discharge process with specific capacities of 120 and 97.4 mAh g^{-1} at 10 mA g^{-1} in lithium-ion and sodium-ion batteries respectively, with stable cycling performance.

Results and Discussion

Red crystalline samples are obtained from the hydrothermal reaction. The material adopts an orthorhombic crystal structure with space group *Cmc2*$_1$.[7b,9] The crystal structure is shown in Figure 1a, b, revealing zigzag $[Fe(C_2O_4)F_2]^{3-}$ chains running along the *x*-axis, where iron octahedra are connected through the oxalate ligand (Figure 1a). Each Fe atom is coordinated by four O atoms (d(Fe–O) = 2.170(7), 2.146(6), 2.194(7), 2.160(6)) and two fluoride atoms ((d(Fe–F) = 1.980(2), 1.995(2)) and the F1-Fe–F2 bond angle is 178.0(4), forming an octahedron.[7b] The Fe is coordinated to two out-of-plane F^- ions, forming a compressed $[FeO_4F_2]$ octahedron (Figure 1b). The adjacent $[FeC_2O_4]^{\infty}$ layers are bridged by sharing fluoride ions to form a three-dimensional framework. There are two potassium sites in the crystal structure, shown as K1 and K2 in Figure 1a, forming two potassium channels. Rietveld refinement of the pristine powder sample was performed to check the phase purity. The refined profile is shown in (Figure 2). Refined atomic parameters were found to match those of the previous single crystal study.[7b]

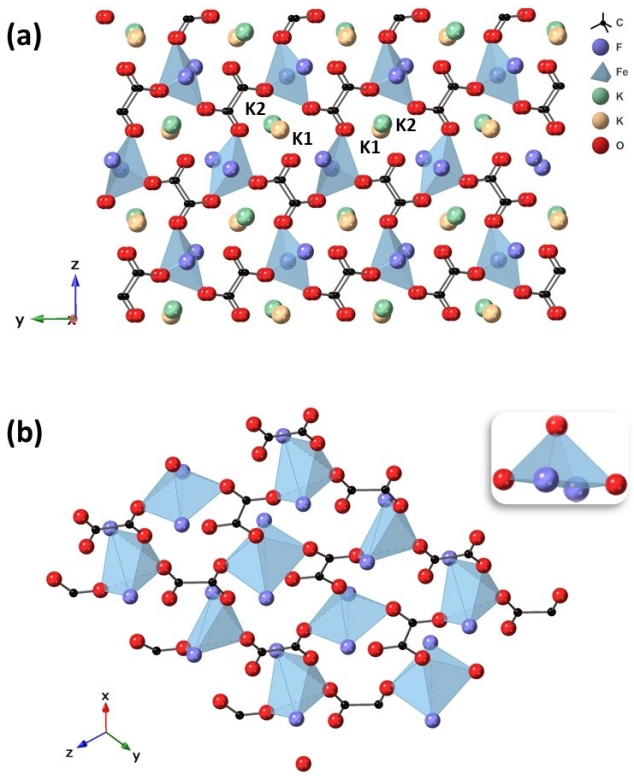

Figure 1. Crystal structure of $KFe(C_2O_4)F$, (a) viewed along the *x*-axis, and (b) $Fe(C_2O_4)_3F_2$ infinite chains, FeO_4F_2 octahedra are shown in the inset.

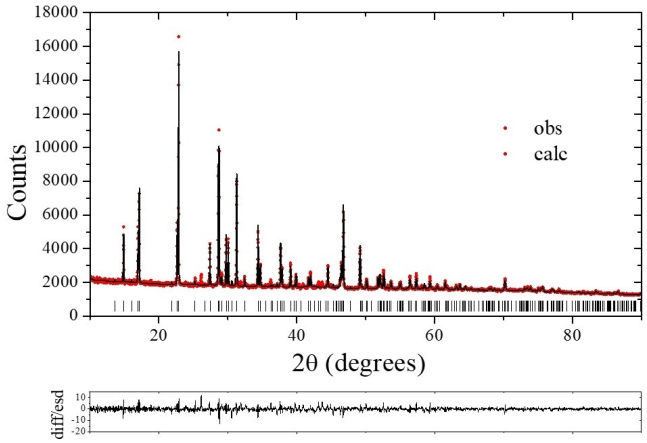

Figure 2. Rietveld refinement analysis of hand-ground, powdered pristine sample at room temperature, lattice parameters are a = 7.7633(1) Å, b = 11.8767(2) Å, c = 10.4206(2) Å, space group *Cmc2*$_1$, wRp = 3.46, χ^2 = 2.21.

The as-prepared crystalline materials were ball-milled for 30 min to reduce the particle size. The low and high magnification SEM images confirm the pristine particles have a particle size of ~65–70 μm (Figure S1a, b), but after ball-milling, this is reduced to ~2–3 μm (Figure S1c. The SEM image of the composite material after ball-milling with carbon is shown in Figure S1d, which reveals the homogeneous distribution of conductive carbon C65 and the sample. To check the elemental distribution of the sample, the energy dispersive X-ray analysis (EDS) and corresponding elemental mapping were performed (Figure S2a, b), revealing a homogeneous distribution of elements throughout the sample. Raman spectroscopy analysis of the pristine sample was also performed (Figure S3) to verify the phase purity of the sample.

Electrochemical characterization in sodium-ion battery (NIB)

The sodium ion storage capability was investigated via cyclic voltammetry (CV) over the voltage window 1.5 to 4.3 V at a sweep rate of 0.1 mV s^{-1} (Figure 3a). The CV curve shows two pairs of redox peaks at 2.9/2.7 and 3.2/3.0 V vs Na^+/Na, which could be ascribed to the stepwise redox reactions of two alkali metal sites in the KFCF electrode.[3d,16] The CV curves are consistent with two redox processes and, following the initial potassium extraction which exhibited a large cell polarisation, were unchanged in the following cycles, with highly reversible electrochemical redox reactions. Figure 3b represents the differential capacity plot of the 3rd, 5th, 10th, and 20th cycles, revealing a broad hump at ~3 V during the sodiation/desodiation process. The differential capacity plots of the 50th, 75th, and 100th cycles also present similar redox behavior, confirming the KFCF electrode's high reversibility in NIBs (Figure S4a). The dQ/dV plot reveals a broad hump instead of two different peaks, which is not infrequent for polyanionic systems.[16] The galvanostatic voltage profiles for the 3rd, 5th, 10th, and 20th cycles at a

© 2023 The Authors. ChemElectroChem published by Wiley-VCH GmbH

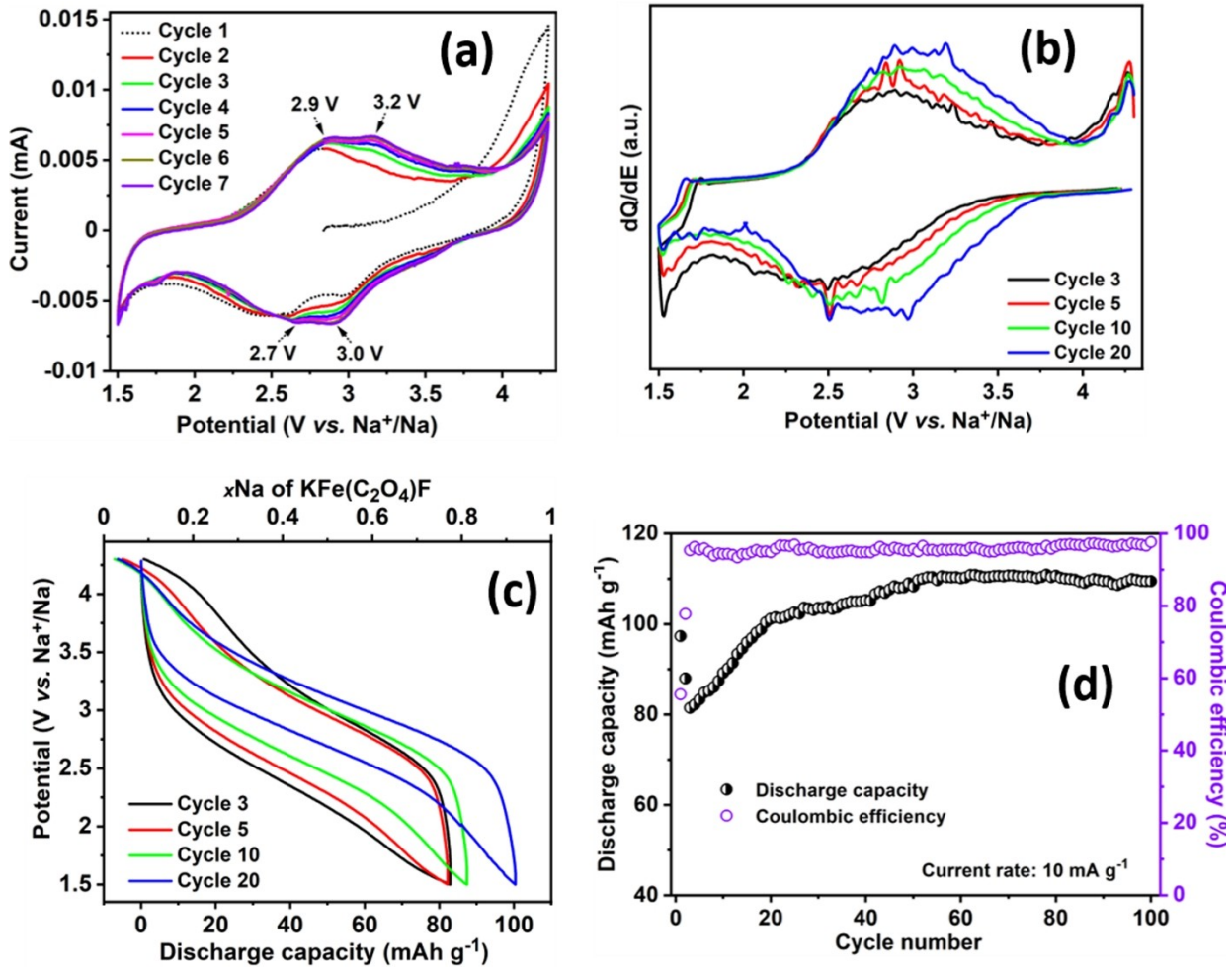

Figure 3. Electrochemical performance in sodium-ion batteries. (a) Cyclic voltammetry curves at 0.1 mV s^{-1} of initial seven cycles, (b) galvanostatic dQ/dE curve, and (c) voltage-capacity plot of 3rd, 5th, 10th, 20th cycles at 1.5–4.3 V voltage window at 10 mA g^{-1} current rate, and (d) evolution of specific capacity with cycles at 10 mA g^{-1} current rate with corresponding coulombic efficiency.

rate of 10 mA g^{-1} over the 1.5-4.3 V voltage window are displayed in figure 3c. A first cycle discharge capacity of ~97.4 mAh g^{-1} was recorded, ~73% of the theoretical capacity (~132.7 mAh g^{-1}). Figure 3d shows the cycling performance with the corresponding coulombic efficiency of the KFCF electrode at a rate of 10 mA g^{-1}. It can be seen that the discharge capacity dropped slightly over the first few cycles before rising after around twenty cycles due to the activation of the electrode with a corresponding increase in the coulombic efficiency (Figure 3d). The increase in the specific capacity is likely to be due to an electrochemical grinding process that improves electronic conductivity and reduces cell polarization of the electrode.[4a] The GCD voltage profiles for the 50th, 75th, and 100th cycles correspond to the region with increased specific capacity equivalent to ~0.85 Na^+ ions exchanged per formula unit during the charge/discharge process (Figure S4b). The specific discharge capacity was observed at ~110 mAh g^{-1} after 100 cycles with ~98% coulombic efficiency (Figure 3d). The rate capability of KFCF at different current densities (10-200 mA g^{-1}) was investigated (Figure S5). From an initial value of ~95 mAh g^{-1} at 10 mA g^{-1}, the discharge capacity dropped to 43 mAh g^{-1} at a rate of 50 mA g^{-1} and around 30 mAh g^{-1} at 200 mA g^{-1}. Once the rate was restored to the initial current density (10 mA g^{-1}), the discharge capacity recovered to ~100 mAh g^{-1}, which reveals good durability despite the moderate rate performance as a cathode material for NIBs.

Electrochemical characterization in lithium-ion battery (LIB)

In addition, we assembled half-cells to investigate the performance as an electrode material in LIBs, as shown in figure 4. As with the NIB investigations the electrochemical properties of KFCF were examined using cyclic voltammetry and galvanostatic experiments. The CV was recorded at a scan rate of 0.1 mV s^{-1} within a 1.8-4.5 V voltage window for seven consecutive cycles (Figure 4a). The differential capacity plot at 2nd, 3rd, 5th, 10th, and 15th reveals a broad process at ~3.2 V and is invariant with increasing cycle number (Figure 4b), demonstrating good reversibility (Figure S6a). The galvanostatic charge-discharge profiles were plotted for the 2nd, 3rd, 5th, 10th, and 15th cycle in between 1.8 to 4.5 V voltage region at a rate of

© 2023 The Authors. ChemElectroChem published by Wiley-VCH GmbH

21960216, 0, Downloaded from https://chemistry-europe.onlinelibrary.wiley.com/doi/10.1002/celc.202300192 by NHS Education for Scotland NES, Edinburgh Central Office, Wiley Online Library on [28/06/2023]. See the Terms and Conditions (https://onlinelibrary.wiley.com/terms-and-conditions) on Wiley Online Library for rules of use; OA articles are governed by the applicable Creative Commons License

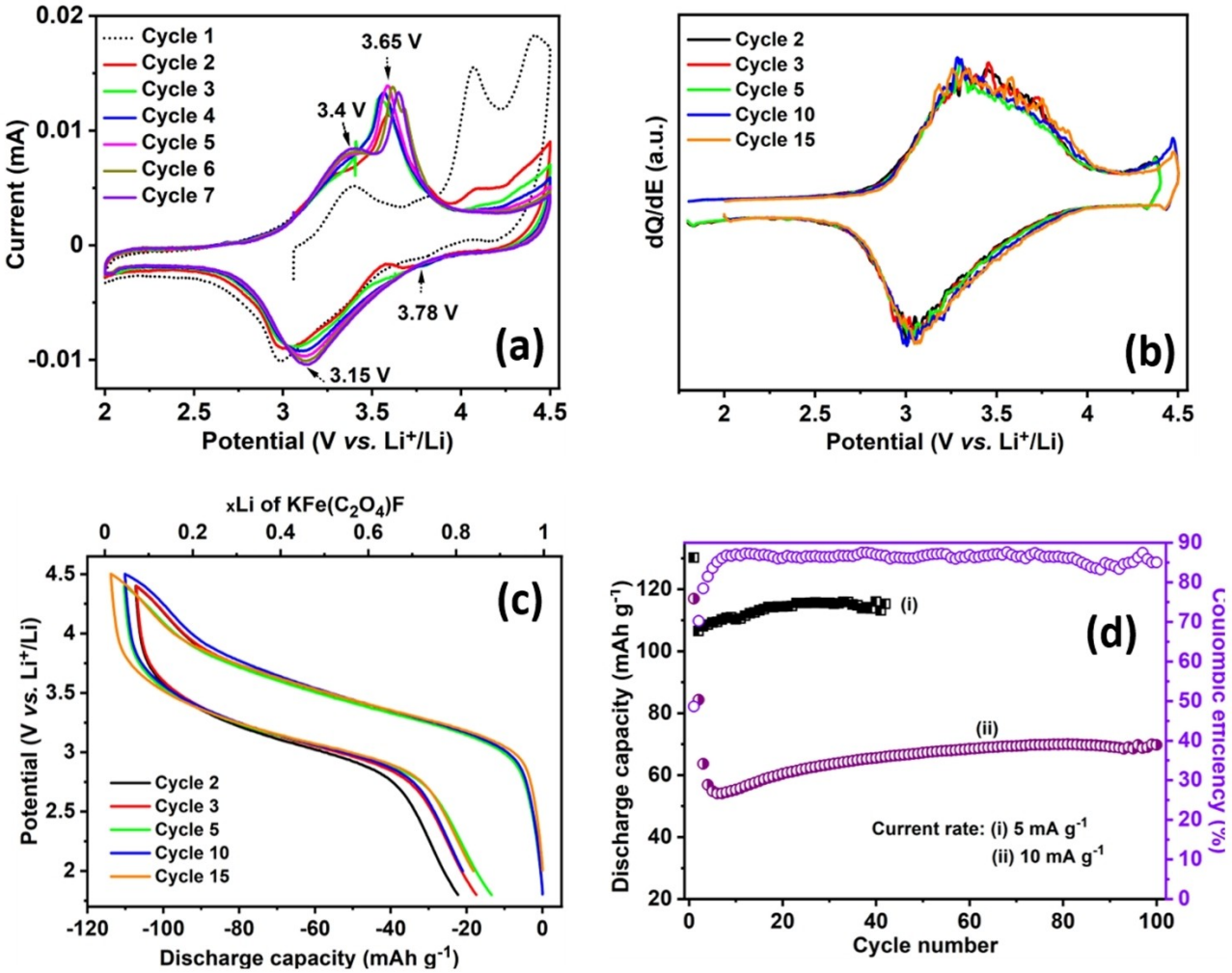

Figure 4. Electrochemical performance as half-cell LIB cathode. (a) Cyclic voltammetry curves at 0.1 mV s^{-1} of initial seven cycles, (b) galvanostatic dQ/dE plot, and (c) voltage-capacity plot of 2nd, 3rd, 5th, 10th, 15th cycles at 1.8–4.5 V voltage window at 5 mA g^{-1} current rate, and (d) cycling stability performances at 5 and 10 mA g^{-1} current rate with coulombic efficiency at 10 mA g^{-1}.

5 mA g^{-1} (Figure 4c), revealing one pseudo plateau on de-lithiation/lithiation, and approximately ~0.96 Li^+ exchanged per formula unit. Similar behavior was also observed at a higher cycle number, confirming the highly reversible redox mechanism (Figure S6b). The cell was cycled at the same voltage window at a 5 mA g^{-1} current rate, and the first cycle discharge capacity was observed at ~130 mAh g^{-1}, ~98% of its theoretical capacity (Figure 4d). The cell shows steady cycling stability with ~116 mAh g^{-1} retained after 40 cycles (~87.4% of its theoretical capacity). In addition, long-term cycling stability was evaluated at 10 mA g^{-1} over the same voltage window (Figure 4d). The first cycle discharge capacity was observed at ~117 mAh g^{-1}. In the subsequent cycles, the discharge capacity initially decreased and then stabilized after a few cycles, delivering ~70 mAh g^{-1} after 100 cycles with ~87% coulombic efficiency.

To explore the local iron oxidation environment during the electrochemical charge and discharge process, *ex-situ* ^{57}Fe Mössbauer spectroscopy measurements were performed at room temperature using coffee bag-type airtight sample holders prepared under an argon atmosphere inside the glove box. Figure 5 shows Mössbauer spectra collected for pristine powder and after five cycles at the charged and discharged states. Each Mössbauer spectrum may be considered the sum of two components (quadrupole doublets), and the refined hyperfine parameters are summarized in Table S1. The KFCF pristine powder's spectrum shows 100% of Fe^{2+} octahedral environments divided into two parts: a principal component with 95% of absorption area having a high quadrupole splitting (2.70 mms) and a minor component with low quadrupole splitting (1.90 mm/s) and both having closer isomer shifts ~1.21–1.26 mm/s (Figure 5a). The Mössbauer spectrum of the pristine material (Figure 5a) shows two contributions. The major contribution (blue line, 95%) corresponds to iron(II) in the crystalline KFCF structure. The minor contribution (red line, 5%) could be attributed to an amorphous iron(II)-based impurity like $Fe(C_2O_4)\cdot 2H_2O$ or potential structural defects similar to those observed in lithium iron sulfates and lithium iron phosphates.[11a,b] The amount of impurity remains unchanged in

© 2023 The Authors. ChemElectroChem published by Wiley-VCH GmbH

21960216, 0, Downloaded from https://chemistry-europe.onlinelibrary.wiley.com/doi/10.1002/celc.202300192 by NHS Education for Scotland NES, Edinburgh Central Office, Wiley Online Library on [28/06/2023]. See the Terms and Conditions (https://onlinelibrary.wiley.com/terms-and-conditions) on Wiley Online Library for rules of use; OA articles are governed by the applicable Creative Commons License

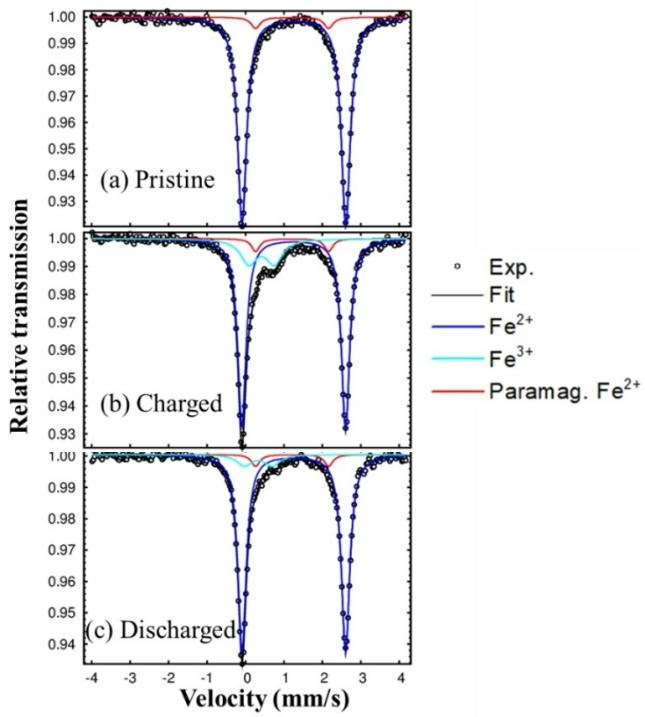

Figure 5. Room temperature Mossbauer spectroscopy of the (a) pristine, (b) sample obtained from a fully charged state at 4.3 V, and (c) fully discharged state up to 1.5 V of the *ex-situ* electrodes after five charge/discharge cycles for NIB.

the charged and discharged states, with negligible impact on the electrochemical process of the main phase.

The slight asymmetry in the main doublet of the Mössbauer spectra could be due to a preferred orientation effect seen in certain sodium oxalates and malonates, or a Goldanskii-Karyagin effect reported for $Fe_3(CO)_{12}$.[12a,b]

The Mössbauer spectra confirm an iron redox process during charge-discharge (Figure 5a-c and Table S1). At the charged state of 4.3 V (Figure 5b), the spectrum exhibits three doublets. The cyan doublet represents iron(III) environments, accounting for 19% of the total iron content at the charged state. In the discharged state (Figure 5c), the spectrum predominantly consists of Fe^{2+} with some residual Fe^{3+} (9%), suggesting incomplete reduction at this voltage. The amount of unreacted material is probably inactive regions of the sample as no binder was used in the sample preparation leading to reduced electrochemical performance. The detailed, refined hyperfine parameters are summarized for three sets of samples in Table S1. Encouraged by the excellent stability of this material as an electrode material in NIB and LIB, we carried out first-principles calculations to further investigate the phenomena occurring during electrochemical cycling.

The lithiated and sodiated phases of $KFe(C_2O_4)F$ were analyzed together with the hypothetical end compound $Fe(C_2O_4)F$, where all alkali ions Na^+ or Li^+ are removed from the unit cell to simulate the initial and final states of our electrochemical studies. These three compounds are stable after geometry optimization with no structural change, whether lithiated or sodiated initial or hypothetical end compound. The calculated lattice parameters are presented in Figures 6a, b, and c and are in good agreement with the XRD experimental data discussed above.

The iron is stable as high-spin Fe^{2+} in both our initial compounds with a calculated magnetic moment of 3.79 μB. In contrast, in the hypothetical end member, is high-spin Fe^{3+} with a calculated magnetic moment of 4.34 μB, in agreement with the Mössbauer analysis. The corresponding electronic

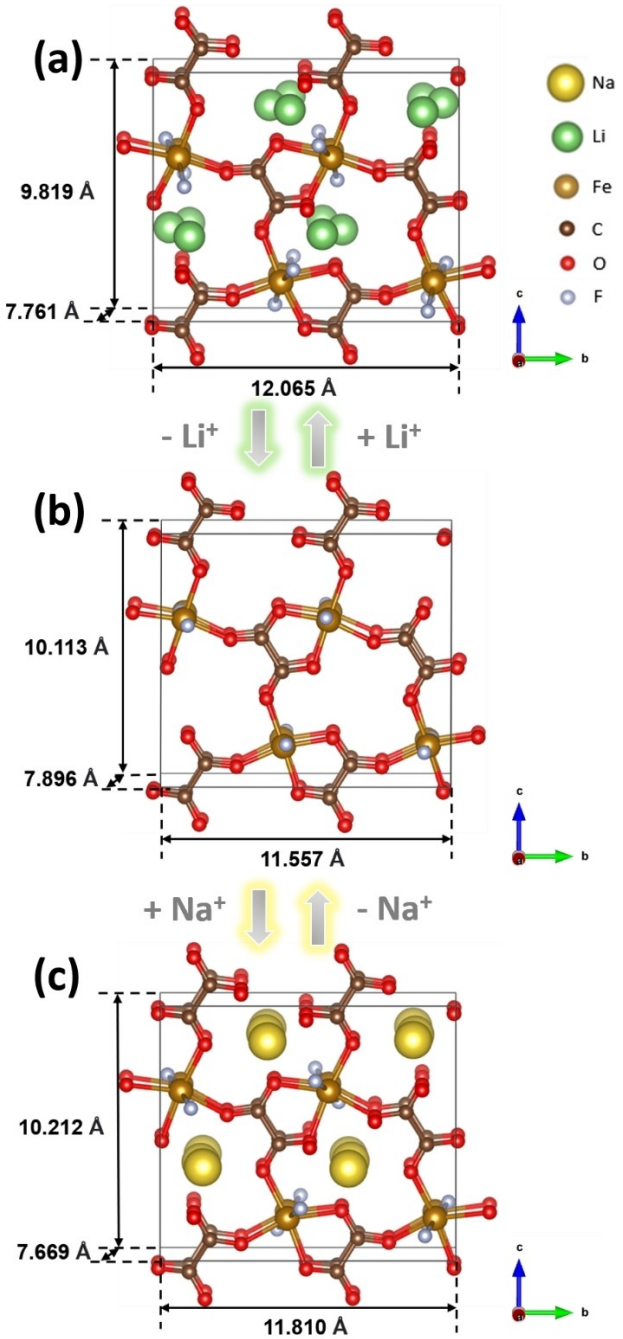

Figure 6. An optimized unit cell of lithiated (a), hypothetical end compound where all alkali ions are removed from the unit cell (b), and sodiated (c) $KFe(C_2O_4)F$ by first-principles calculations with their corresponding cell parameters.

© 2023 The Authors. ChemElectroChem published by Wiley-VCH GmbH

21960216, 0, Downloaded from https://chemistry-europe.onlinelibrary.wiley.com/doi/10.1002/celc.202300192 by NHS Education for Scotland NES, Edinburgh Central Office, Wiley Online Library on [28/06/2023]. See the Terms and Conditions (https://onlinelibrary.wiley.com/terms-and-conditions) on Wiley Online Library for rules of use; OA articles are governed by the applicable Creative Commons License

density of states of lithiated and sodiated $KFe(C_2O_4)F$ and $Fe(C_2O_4)F$ are shown in Figures 7a, b, and c in the antiferromagnetic spin configuration. The lithiated and sodiated compounds have calculated band gaps of 1.60 and 1.32 eV, respectively, which is smaller than that of many other polyanionic compounds, such as $Na_2Fe(C_2O_4)F_2$ (1.94 eV),[7a] $Na_2Fe_2(C_2O_4)_3 \cdot 2H_2O$ (2.34 eV),[4a] $LiFePO_4$ (2.93 eV),[13a] and $LiFeSO_4F$ (3.60 eV).[13b] These reduced band gaps are beneficial to electron transport in the materials. For example, the hypothetical end compound $Fe(C_2O_4)F$ has a calculated band gap of 1.18 eV.

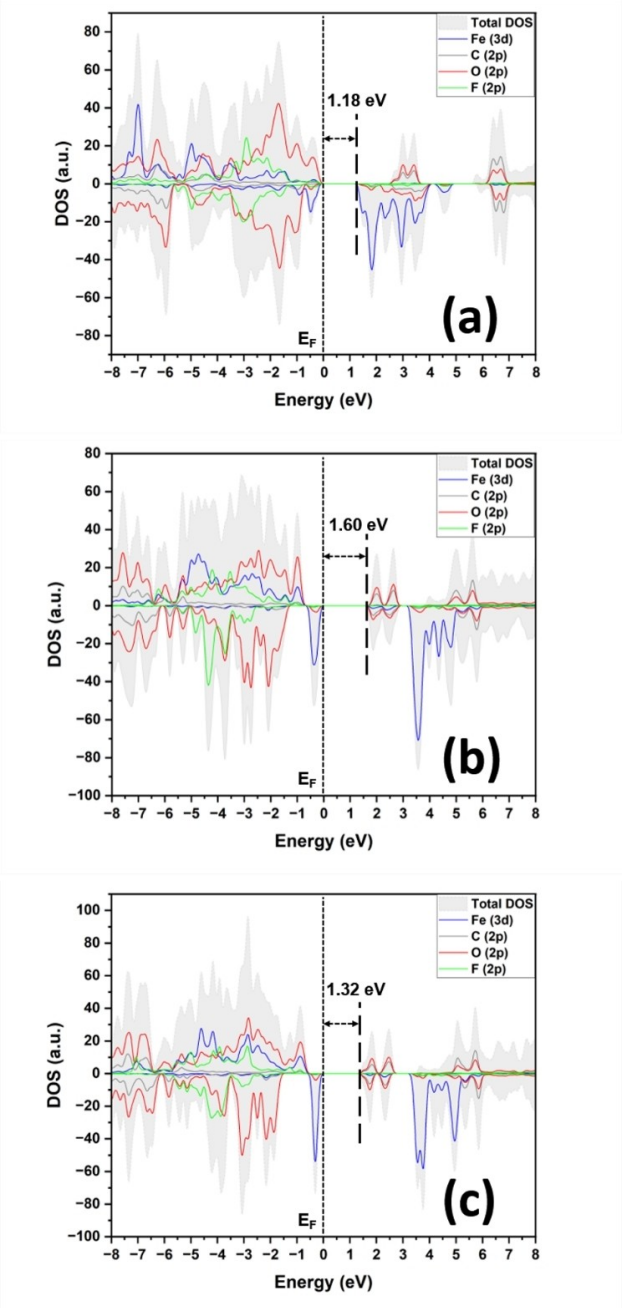

Figure 7. Total and projected density of states (DOS) onto the Fe (3d), C (2p), O (2p), and F(2p) orbitals of lithiated (a), hypothetical end compound (b), and sodiated (c). The Fermi level E_F (at 0 eV) is set to the highest occupied state.

The calculated electronic structure near the band edges gives information about the intrinsic redox mechanism.[16] For example, it can be seen from Figures 6d and f that the top of the valence band of lithiated and sodiated $KFe(C_2O_4)F$ is mainly composed of the highly localized Fe 3d states. In contrast, the bottom of the conduction band is predominantly C and O 2p states.

Alkali-ion extraction from the cathode involves removing electrons from the highest occupied states, and the spin-up orbitals shift to deeper levels. The spin-down orbitals move to higher levels above the Fermi level E_F, allowing oxidation at the Fe^{2+} sites. As a result, the top of the valence band of $Fe(C_2O_4)F$ (Figure 6e) is predominantly composed of O 2p states, whereas spin-down Fe 3d states mainly occupy the bottom of the conduction band. As alkali-ion (re)insertion involves adding electrons to the lowest unoccupied states, this process occurs by reducing the Fe^{3+} sites. These results are consistent with the Fe^{3+}/Fe^{2+} reversible redox reactions observed with Mössbauer spectroscopy.

Conclusions

We successfully developed a polyanionic fluoro-oxalate positive electrode material ($KFe(C_2O_4)F$) via a simple hydrothermal technique for LIB/NIB application. It delivers 115 and 65 mAh g^{-1} specific discharge capacity at cycling rates or 5 and 10 mA g^{-1} respectively, when cycled over the 1.8--4.5 V potential window during lithiation/delithiation mechanism. In addition, in sodium-ion batteries, 97.4 mAh g^{-1} (74% of its theoretical capacity) specific discharge capacity at 10 mA g^{-1} was noted at 1.5–4.3 V potential window, and it reaches ~110 mAh g^{-1} reversible capacity with 99% coulombic efficiency after 100 cycles. *Ex-situ* Mössbauer spectroscopy and first-principles calculations validated the iron redox (Fe^{2+}/Fe^{3+}) activity of the material.

Experimental Section

Synthesis of $KFe(C_2O_4)F$

$KFe(C_2O_4)F$ crystals were synthesized via a conventional hydrothermal technique.[8,9] All the chemicals were used without further purification. $Fe(C_2O_4) \cdot 2H_2O$ (Merck, Germany 99%), $C_2H_2O_4$ (Merck, Germany 99%), KBF_4 (Merck, Germany 99%), and K_2CO_3 (Merck, Germany 99%) in a 1:3:2:4 molar ratio were placed in a 23 mL Teflon-lined autoclave with 1 mL of ethylene glycol (Sigma-Aldrich, anhydrous, 99.8%). The sealed autoclave was placed in an oven at 160 °C for 48 h, after which it was manually removed and cooled to room temperature. The orange crystals were washed several times with distilled water and acetone. Finally, the product was dried in an oven at 60 °C for 4 h.

Material characterization

The orange crystalline samples were hand ground, and powder X-ray diffraction (PXRD) was performed using a Stoe STADIP diffractometer with Mo $K\alpha_1$ radiation ($\lambda = 0.70930$ Å) in the 2θ

© 2023 The Authors. ChemElectroChem published by Wiley-VCH GmbH

21960216, 0, Downloaded from https://chemistry-europe.onlinelibrary.wiley.com/doi/10.1002/celc.202300192 by NHS Education for Scotland NES, Edinburgh Central Office, Wiley Online Library on [28/06/2023]. See the Terms and Conditions (https://onlinelibrary.wiley.com/terms-and-conditions) on Wiley Online Library for rules of use; OA articles are governed by the applicable Creative Commons License

range 3–55°, operating in Debye-Scherrer mode with a position sensitive Mythen linear detector. The data were recorded at room temperature using a capillary (0.5 mm diameter). The phase purity of the sample was verified by Rietveld refinement using the GSAS II package.[10] A fixed structural model obtained from the single crystal study was used to refine the PXRD data, with spherical harmonics used to model the preferred orientation. A JEOL JSM-6700F scanning electron microscope (SEM) was used to record the microstructures and EDS elemental analysis of the pristine, ball-milled, and composite samples. The secondary images of all samples were recorded by applying a tungsten filament electron source at 15 kV accelerating voltage. Atomic number contrast imaging was recorded by applying a retractable backscattered electron detector. A Renishaw inVia Qontor confocal Raman microscope was used to measure Raman spectra using a 532 nm laser.

Electrochemical characterization

The electrochemical measurements were performed on pellet electrodes. Firstly, 0.60 g of active material was ball-milled for 30 min to reduce the particle size using a Fritsch Pulverisette 8 mill. After that, 0.30 g super C65 conductive carbon black (Imerys) was added, followed by another 30 min ball-milling. Finally, the composite powders were combined with 0.1 g polytetrafluoroethylene (PTFE) binder by hand grinding to obtain a homogeneous composite material. The self-standing 13 mm diameter pellet electrodes were assembled at a pressure of ~4 tonnes cm^{-2} using a hydraulic press. The electrodes, with an average active mass of ~5 mg, were dried overnight (~12 h) in a vacuum oven before assembling coin cells. CR2325 type coin cells (NRC Canada) were fabricated in an Ar-filled glovebox using sodium metal as the counter electrode, a glass fiber separator (Whatman, GF/F) and 1 M $NaClO_4$ in propylene carbonate with 3% fluoroethylene carbonate additive as electrolyte for NIB. The LIB coin cells were fabricated using lithium metal as a counter electrode and commercial LP30 (1 M $LiPF_6$ in ethylene carbonate: dimethyl carbonate = 1:1, Merck) as electrolytes. The half-cells were tested by galvanostatic cycling in the potential window of 1.5–4.3 V for NIB and 1.8–4.5 V for LIB using a Biologic Macpile II system at a current rate of 10 mA g^{-1}.

Mössbauer Spectroscopy measurements

Room temperature Mössbauer spectra of the pristine material and material extracted after five cycles in both charged and discharged state were recorded on absorbers prepared under argon (coffee bags). The *ex-situ* Mössbauer spectroscopy samples were prepared by assembling Swagelok cells. After five cycles of charge/discharge, the cells were opened inside the glove box and washed three times with dimethyl carbonate (DMC), where each absorber contains 30–40 mg cm^{-2} active material. The spectrometer activates in the constant acceleration transmission geometry. The ^{57}Co/Rd, 850 MBq, γ-ray source was maintained at room temperature. The pure α-Fe standard was used to calibrate the isomer shift scale. The obtained spectra were fitted using a least-squares method and a combination of Lorentzian lines with the MOSFIT program.

Theoretical calculations

All the calculations were performed under the Vienna Ab initio Simulation Package (VASP) based on the spin-polarized Density Functional Theory (DFT).[16a,b] The Perdew, Burke, and Ernzerhof (PBE)[17] functional of the Generalized-Gradient Approximation (GGA) and the Projector Augmented Wave (PAW) method were used.[16a,b] The Hubbard correction[18] with an effective U value of 4.0 eV was applied for the Fe 3d states to correct the on-site Coulomb repulsion.[19] The energy cut-off was set at 520 eV, and spin polarization was included in all calculations. For the geometry optimizations and total-energy calculations, we used a Γ-centered 6×4×4 k-point mesh. A denser k-point mesh of 9×6×6 is used in calculations to obtain the electronic density of states. The criterion for energy convergence was set to 10–5 eV.

Supporting Information

The supporting information contains SEM images of pristine, ball-milled and composite samples for $KFe(C_2O_4)F$. SEM-EDS and corresponding mapping for KFCF pristine sample. Raman spectroscopy plot for pristine KFCF. Galvanostatic dQ/dV plots and related voltage-capacity profiles for different cycles for LIB and NIB. Rate performance for NIB electrode. Mössbauer analysis data table for charge and discharge states.

Acknowledgements

The authors want to thank EPSRC (EP/R030472/1) and the Faraday Institution (FIRG018) for their financial support. In addition, AGM wishes to thank the Faraday Institution for financial support and training (Grant number FITG033). The authors also thank EPSRC Light Element Analysis Facility Grant EP/T019298/1 and the EPSRC Strategic Equipment Resource Grant EP/R023751/1.

Conflict of Interests

The authors declare no conflict of interest.

Data Availability Statement

The data that support the findings of this study are available from the corresponding author upon reasonable request.

Keywords: cathode materials · electrochemistry · Na-ion/Li-ion · oxalate · rechargeable battery

[1] J–M Tarascon, M. Armand, *Nature* **2001**, *414*, 359–367.
[2] V. Palomares, M. Casas-Cabanas, E. Castillo-Martínez, M. H. Han, T. Rojo, *Energy Environ. Sci.* **2013**, *6*, 2312–2337.
[3] a) M. H. Han, E. Gonzalo, G. Singh, T. Rojo, *Energy Environ. Sci.* **2015**, *8*, 81–102; b) A. Kanwade, S. Gupta, A. Kankane, A. Srivastava, S. C. Yadav, P. M. Shirage, *Sustain. Energy Fuels* **2022**, *6*, 3114–47; c) M. Chen, W. Hua, J. Xiao, D. Cortie, W. Chen, E. Wang, Z. Hu, Q. Gu, X. Wang, S. Indris, S. L. Chou, S. X. Dou, *Nat. Commun.* **2019**, *10*, 1–11; d) W. Pan, W. Guan, S. Liu, B. Xu Bin, C. Liang, H. Pan, M. Yan, Y. Jiang, *J. Mater. Chem. A* **2019**, *7*, 13197–204; e) S. Li, J. Guo, Z. Ye, X. Zhao, S. Wu, J. X. Mi, C. Z. Wang, Z. Gong, M. J. McDonald, Z. Zhu, K. M. Ho, Y. Yang, *ACS Appl. Mater. Interfaces* **2016**, *8*, 17233–8; f) P. Barpanda, L. Lander, S. I. Nishimura, A. Yamada, *Adv. Energy Mater.* **2018**, *8*, 1703055; g) Y. Wu, X. Meng, L. Yan, Q. Kang, H. Du, C. Wan, M. Fan, T. Ma, *J. Mater. Chem. A* **2022**, *10*, 21816–37.
[4] a) W. Yao, M. T. Sougrati, K. Hoang, J. Hui, P. Lightfoot, A. R. Armstrong, *Chem. Mater.* **2017**, *29*, 9095–101; b) W. Yao, A. R. Armstrong, X. Zhou, M. T. Sougrati, P. Kidkhunthod, S. Tunmee, C. Sun, S. Sattayaporn, P.

© 2023 The Authors. ChemElectroChem published by Wiley-VCH GmbH

21960216, 0, Downloaded from https://chemistry-europe.onlinelibrary.wiley.com/doi/10.1002/celc.202300192 by NHS Education for Scotland NES, Edinburgh Central Office, Wiley Online Library on [28/06/2023]. See the Terms and Conditions (https://onlinelibrary.wiley.com/terms-and-conditions) on Wiley Online Library for rules of use; OA articles are governed by the applicable Creative Commons License

Lightfoot, B. Ji, C. Jiang, N. Wu, Y. Tang, H. M. Cheng, *Nat. Commun.* **2019**, *10*, 1–9; c) A. Pramanik, A. G. Manche, M. T. Sougrati, A. V. Chadwick, P. Lightfoot, A. R. Armstrong, *Chem. Mater.* **2023**, *35*, 2600–2611; d) A. Pramanik, A. G. Manche, R. Clulow, P. Lightfoot, A. R. Armstrong, *Dalton Trans.* **2022**, *51*, 12467–75; e) A. Pramanik, A. J. Bradford, S. L. Lee, P. Lightfoot, A. R. Armstrong, *J. Phys. Mater.* **2021**, *4*, 024004; f) T. Son, W. Yao, P. Kiadkhunthod, Y. Zheng, N. Wu, X. Zhou, S. Tunmee, S. Sattayaporn, Y. Tang, *Angew. Chem. Int. Ed.* **2020**, *59*, 740–745.

[5] N Pinna, N. Goubard-Bretesché, *Adv. Energy Mater.* **2021**, *11*, 2002971.

[6] a) N. Goubard-Bretesché, E. Kemnitz, N. Pinna, *Mater. Chem. Front.* **2019**, *3*, 2164–74; b) X. Li, S. Jiang, S. Li, J. Yao, Y. Zhao, T. Bashir, S. Zhou, S. Yang, W. Li, W. Zhu, T. Liu, J. Zhao, L. Gao, *J. Mater. Chem. A* **2021**, *9*, 11827–38; c) P. Barpanda, J. M. Tarascon, *Lithium Batteries*, John Wiley & Sons, Ltd, **2013**, 127–60.

[7] a) W. Yao, M. T. Sougrati, K. Hoang, J. Hui, P. Lightfoot, A. R. Armstrong, *Chem. Mater.* **2017**, *29*, 2167–72; b) W. Yao, L. Clark, M. Xia, T. Li, S. L. Lee, P. Lightfoot, *Chem. Mater.* **2017**, *29*, 6616–20.

[8] B. Ji, W. Yao, Y. Zheng, P. Kidkhunthod, X. Zhou, S. Tunmee, S. Sattayaporn, H. M. Cheng, H. He, Y. Tang, *Nat. Commun.* **2020**, *11*, 1–10.

[9] K. Tustain, L. Farrar, W. Yao, P. Lightfoot, I. Da Silva, M. T. F. Telling, L. Clark, *Inorg. Chem.* **2019**, *58*, 11971–7.

[10] W. Tang, X. Song, Y. Du, C. Peng, M. Lin, S. Xi, B. Tian, J. Zheng, Y. Wu, F. Pan, K. P. Loh, *J. Mater. Chem. A* **2016**, *4*, 4882–92.

[11] a) L. Lander, M. Reynaud, M. T. Sougrati, C. Laberty-Robert, R. J. Messinger, J. M. Tarascon, *Chem. Mater.* **2014**, *26*, 4178–4189; b) R. Amisse, M. T. Sougrati, L. Stievano, C. Davoisne, G. Draz, B. Budic, R. Dominko, C. Masquelier, *Chem. Mater.* **2015**, *27*, 4261–4273.

[12] a) H. Ahouari, G. Rousse, Y. Klein, J. N. Chotard, M. T. Sougrati, N. Recham, J. M. Tarascon, *Solid State Sci.* **2015**, *42*, 6–13; b) F. Grandjean, G. J. Long, C. G. Benson, U. Russo, *Hyperfine Interact.* **1988**, *40*, 299–302.

[13] a) L. Yang, Y. Tian, J. Chen, J. Gao, Z. Long, W. Deng, G. Zou, H. Hou, X. Ji, *J. Mater. Chem. A* **2021**, *43*, 24686–94; b) S. Adams, R. P. Rao, *Solid State Ionics* **2011**, *184*, 57–61.

[14] K. Hoang, *Phys. Rev. Appl.* **2015**, *3*, 024013.

[15] R. B. Von Dreele, *J. Appl. Crystallogr.* **1997**, *30*, 517.

[16] a) P. E. Blöchl, *Phys. Rev. B* **1994**, *50*, 17953; b) D. Kresse, G. Joubert, *Phys. Rev. B: Condens. Matter Mater. Phys.* **1999**, *59*, 1758–1775.

[17] J. P. Perdew, K. Burke, M. Ernzerhof, *Phys. Rev. Lett.* **1996**, *77*, 3865.

[18] S. L. Dudarev, G. A. Botton, S. Y. Savrasov, C. J. Humphreys, A. P. Sutton, *Phys. Rev. B* **1998**, *57*, 1505.

[19] L. Wang, T. Maxisch, G. Ceder, *Phys. Rev. B* **2006**, *73*, 195107.

Manuscript received: May 3, 2023
Revised manuscript received: June 18, 2023
Version of record online: ■■, ■■

© 2023 The Authors. ChemElectroChem published by Wiley-VCH GmbH

21960216, 0, Downloaded from https://chemistry-europe.onlinelibrary.wiley.com/doi/10.1002/celc.202300192 by NHS Education for Scotland NES, Edinburgh Central Office, Wiley Online Library on [28/06/2023]. See the Terms and Conditions (https://onlinelibrary.wiley.com/terms-and-conditions) on Wiley Online Library for rules of use; OA articles are governed by the applicable Creative Commons License

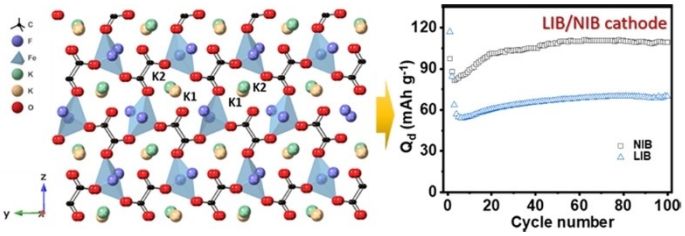

A hydrothermal method is used for preparing $K_2Fe(C_2O_4)_2$ (KFCF), a new iron-based material. It demonstrates promising reversible lithium and sodium insertion properties as a **cathode material**. The material delivers a first-cycle discharge capacity of 120 mAh g^{-1} at ~3.3 V (Li^+/Li) and 97.4 mAh g^{-1} at ~3.0 V (Na^+/Na) in Lithium-ion battery (LIB) and Sodium-ion battery (NIB), respectively. The reversible Fe^{2+}/Fe^{3+} redox is confirmed by ex-situ Mössbauer spectroscopy and first-principles calculations, making KFCF a potential candidate for new electrode materials.

*Dr. A. Pramanik, A. G. Manche, M. T. Smeaton, Dr. M.-T. Sougrati, Prof. P. Lightfoot, Dr. A. R. Armstrong**

1 – 9

$KFe(C_2O_4)F$: A Fluoro-oxalate Cathode Material for Li/Na-Ion Batteries

21960216, 0, Downloaded from https://chemistry-europe.onlinelibrary.wiley.com/doi/10.1002/celc.202300192 by NHS Education for Scotland NES, Edinburgh Central Office, Wiley Online Library on [28/06/2023]. See the Terms and Conditions (https://onlinelibrary.wiley.com/terms-and-conditions) on Wiley Online Library for rules of use; OA articles are governed by the applicable Creative Commons License